

A Universal Variational Framework for Sparsity-Based Image Inpainting

Fang Li and Tiejiong Zeng

Abstract—In this paper, we extend an existing universal variational framework for image inpainting with new numerical algorithms. Given certain regularization operator Φ and denoting u the latent image, the basic model is to minimize the ℓ_p , ($p = 0, 1$) norm of Φu preserving the pixel values outside the inpainting region. Utilizing the operator splitting technique, the original problem can be approximated by a new problem with extra variable. With the alternating minimization method, the new problem can be decomposed as two subproblems with exact solutions. There are many choices for Φ in our approach such as gradient operator, wavelet transform, framelet transform, or other tight frames. Moreover, with slight modification, we can decouple our framework into two relatively independent parts: 1) denoising and 2) linear combination. Therefore, we can take any denoising method, including BM3D filter in the denoising step. The numerical experiments on various image inpainting tasks, such as scratch and text removal, randomly missing pixel filling, and block completion, clearly demonstrate the super performance of the proposed methods. Furthermore, the theoretical convergence of the proposed algorithms is proved.

Index Terms—Image inpainting, diffusion, exemplar, sparsity, frame, shrinkage.

I. INTRODUCTION

IMAGE inpainting is an important topic in the field of computer vision and image processing, which aims to filling-in the missing pixels in an incomplete observed image. Image inpainting has wide applications such as text and scratch removal for ancient drawings or old pictures, recovering lost blocks or pixels damaged during image coding and transmission, removal of objects in photography or films for special effects. Ideally, the inpainted image should possess structures and texture patterns consistent with the given data. Indeed, it should be natural for human eyes.

Many useful techniques have been proposed in recent years to address the task of image inpainting, which can be roughly classified into two categories: pixel based method and exemplar based method. In pixel based method, the fundamental

procedure is conducted on the level of pixel. In contrast, exemplar based method considers an exemplar (or a patch) as a fundamental processing element.

Pixel based method includes variational and partial differential equation (PDE) based method and sparsity based method. In PDE method, the missing region is filled by diffusing the image information from the known region into the missing region. The pioneered work of Bertalmio *et al.* [1] filled in the holes by propagating information from the outside of the inpainting region along isophotes (i.e., level lines of equal gray values). Ballester *et al.* [2] proposed to propagate both image gray values and image gradient vector field into the holes of missing data. Chan and Shen [3] developed a total variation (TV) model for local non-texture inpainting, then derived the diffusion equation as the negative gradient flow of the Euler-Lagrange equation. Taking account of geometric information of isophotes (i.e. curvature) in the total variation diffusion equation, this method can connect some broken edges. Masnou and Morel [4], and Shen *et al.* [5] studied the variational inpainting models based on Euler elastica in which curvature is also involved. Grossauer *et al.* [6] used the complex Ginzburg-Landau equation for digital inpainting in 2D and 3D. Moreover, Bertozzi *et al.* [7], Burger *et al.* [8] adopted the Cahn-Hilliard equation for inpainting binary image and gray value image. In [9], Tai *et al.* proposed to first propagate the isophote directions into the inpainting region by TV-Stokes equation and then restore the image along the constructed directions. Numerically, these PDE methods are implemented with heat flow method which is relatively slow. Recently, some fast numerical methods have been introduced in image inpainting. Li *et al.* [10] addressed a fast numerical algorithm to solving TV inpainting model. Tai *et al.* [11] proposed an efficient algorithm for Euler elastica inpainting model. Marz *et al.* [12], [13] proposed fast inpainting method based on coherence transportation. Ng *et al.* [14] proposed to use the augmented Lagrangian method to solve the coupled problem of blurred image decomposition and inpainting. These PDE based inpainting techniques achieve good results for non-texture (cartoon) image with local thin missing region. However, for larger missing region, the structures in the image fail to propagate into the missing region and blur effect occurs.

Recently, the sparsity based method has been studied for image inpainting. The basic idea here is to represent image by sparse combination of a set of transforms (e.g., wavelet, contourlet, DCT, tight frame, etc.), and then the missing pixels can be filled by adaptively updating the sparse representation. Cai *et al.* [15] used wavelet tight frame. Chan *et al.* [16] applied the Harr-wavelet. Guleryuz *et al.* [17] proposed an

Manuscript received September 13, 2013; revised May 23, 2014; accepted August 2, 2014. Date of publication August 7, 2014; date of current version August 29, 2014. This work was supported in part by the 973 Program under Grant 2011CB707104, in part by the National Science Foundation of China under Grant 11001082 and Grant 11271049, in part by the Research Grants Council (RGC), under Grant 211710 and Grant 211911, and in part by the Research Fellowship Grant, Hong Kong Baptist University, Hong Kong. The associate editor coordinating the review of this manuscript and approving it for publication was Prof. Damon M. Chandler.

F. Li is with the Department of Mathematics, East China Normal University, Shanghai 200241, China (e-mail: fli@math.ecnu.edu.cn).

T. Zeng is with the Department of Mathematics, Hong Kong Baptist University, Hong Kong (e-mail: zeng@hkbu.edu.hk).

Color versions of one or more of the figures in this paper are available online at <http://ieeexplore.ieee.org>.

Digital Object Identifier 10.1109/TIP.2014.2346030

image inpainting algorithm based on adaptive sparse reconstruction and iterated denoising. Elad *et al.* [18] considered an image inpainting method using morphological component analysis (MCA), in which the observed image is decomposed into texture and cartoon layers such that each layer can be sparsely represented by a dictionary. This approach is effective in filling-in regions with both structures and textures, especially in missing block completion. For large missing region, similar as the PDE based method, it brings blurring effect. Fadili *et al.* [19] proposed an expectation-conditional maximization (ECM) algorithm for image inpainting and zooming based on sparse representation. Yu *et al.* [20] utilized the structured sparsity based method for image zooming which provides state of the art results. Ram *et al.* [21] developed an image denoising and inpainting method using smooth ordering of its patches (SOP).

In the exemplar based inpainting method, the image information in the known region propagates into the missing region patch by patch. The texture synthesis method such as [22] is good at pure texture pattern inpainting. As mentioned above, PDE based method is good at structure inpainting. However, natural image usually contains both structure and texture, substantial works are then needed. Bertalmio *et al.* [23] proposed to decompose the observed image into structure component and texture component, and then inpaint the two components with PDE method and texture synthesis method separately. This overcomes the smooth effect of PDE method and can inpaint relatively larger areas. Criminisi *et al.* [24] designed an exemplar-based inpainting algorithm by copying the optimal patch and pasting into the missing region one by one. The inpainting order (patch priority) and the choice of optimal patch are thus crucial in this method. Based on non-local mean filter, Wong [25] proposed to chose optimal patch as weighted average of its non-local neighborhood. Xu and Sun [26] considered new patch priority using structure sparsity and chose optimal patch as a sparse combination of the similar patches. A geometrically guided exemplar based inpainting was given in [27] by Cao *et al.* Arias *et al.* [28] proposed variational framework for exemplar based image inpainting which combines the local and non-local methods. Compared with pixel based method, the exemplar based method is efficient in large missing region inpainting and object removal. However, exemplar based method is sensitive to patch size and for small missing region, the result is not so good.

In this paper, we extend an existing universal variational framework for image inpainting and propose new numerical algorithms. By utilizing operator splitting method, we get a relaxed minimization problem with two variables. The two variables can be easily solved by alternating minimization method. Then we get a universal framework called iterative coupled inpainting algorithm. For some special transform Φ , to increase the stability of the algorithm, we make some modification and get the iterative decoupled inpainting algorithm. In the decoupled algorithm, the iteration scheme is decoupled into two steps which come from minimizing different energies. One step is denoising, the other is linear combination of the denoised image with the observed image. In such a framework, denoising step becomes crucial. Since image denoising is far

more widely studied than image inpainting, we can take use of any denoising method in the first step. For example, the over complete dictionary learning based denoising method and BM3D denoising method, which are the two state-of-the-art denoising methods. By applying the best denoising method in the first step, we can get state-of-the-art inpainting results. We remark that the idea of decoupling is inspired from [43], in which image deblurring problem is decoupled into denoising and deblurring steps and state-of-the-art result is achieved.

The paper is organized as follows. In Section II, we propose the universal model and algorithms for image inpainting. Some mathematical results are proved in Section III. The experiments and comparisons with the previous algorithms are performed in Section IV. Finally, we conclude this work in Section V.

II. PROPOSED METHOD

In this section, we propose the algorithms for a universal image inpainting model. Theoretically we prove the convergence of the proposed algorithm.

A. Inpainting Model

Let us denote images as vectors in R^N by concatenating their columns. Assume that $\Omega = \{1, 2, \dots, N\}$ is the image domain, the nonempty set $\Lambda \subsetneq \Omega$ is the known region, and Ω/Λ is the inpainting region where the information is missing. Let f be the given observed image defined on Λ , and u be the latent image defined on Ω . We first extend f on domain Ω by cubic interpolation.

Assume that $\Phi \in R^{M \times N}$ is a given transform matrix corresponding to some operator, $\mathcal{P}_\Lambda \in R^{N \times N}$ is the diagonal matrix with diagonal entries 1 for the indices in Λ and 0 otherwise. To fill-in the missing region, we study the following classical model

$$\min_u \|\Phi u\|_p + \frac{\lambda}{2} \|\mathcal{P}_\Lambda(u - f)\|_2^2, \quad (1)$$

where λ is a positive parameter, $p \geq 0$. The transformed coefficients $\Phi u \in R^M$ is a column vector, such that its ℓ_p norm is well defined.

Let us give some interpretation of the model. The first term can be seen as regularization term which requires that the coefficient $|\Phi u|$ has small ℓ_p norm. When $p = 0$, $\|\Phi u\|_0$ is defined as the number of nonzero elements in Φu . Smaller ℓ_0 norm means that the representation of Φu is more sparse. When $p > 0$, $\|\Phi u\|_p$ denotes ℓ_p norm, which can be seen as a relaxation of ℓ_0 norm and is widely studied in the literature. So the first term can be interpreted as requiring sparse representation of u by Φ . If $\Lambda = \Omega$, model (1) becomes denoising model for Gaussian noise. For example, if $\Phi = \nabla$, model (1) is the Rudin-Osher-Fatemi (ROF) denoising model [29]. The corresponding fast numerical algorithms are widely studied [30], [31]. If Φ is wavelet transform, model (1) is the wavelet shrinkage denoising method [32]. We can set Φ as other tight frame transforms such as DCT [33], curvelet [34], contourlet [35], framelet [36], in which denoising can also be done by shrinkage.

Actually, there is a wide range of choices for the regularization operator ϕ in the existing literature.

The second term in model (1) is a data fitting term, which requires that u should be close to f in the known region Λ ,

$$u(x) = f(x), \quad \forall x \in \Lambda,$$

or equivalently,

$$\mathcal{P}_\Lambda u = \mathcal{P}_\Lambda f. \quad (2)$$

This is called hard constraint. Actually, the fidelity term in model (1) is a relaxation of the hard constraint. Similar fidelity terms have been used in [3], [7], and [8].

Remark that the hard constraint can also be used in our framework. However, the relaxed version makes the model more flexible. For example, it can handle image denoising and deblurring simultaneously. Moreover, it can be easily generalized to other problem such as deblurring and inpainting,

$$\min_u \|\Phi u\|_p + \frac{\lambda}{2} \|\mathcal{P}_\Lambda(Au - f)\|_2^2 \quad (3)$$

where A is a known blur operator.

B. Algorithm ICI

In the numerical aspect, we use some operator splitting technique [37] to solve model (1). Firstly, we add a new variable w to substitute the transformed coefficients Φu , and rewrite the model as

$$\min_{u,w} \|w\|_p + \frac{\lambda}{2} \|\mathcal{P}_\Lambda(u - f)\|_2^2, \quad s.t. \quad \Phi u = w. \quad (4)$$

Then we get rid of the constraint by quadratic penalty method and get the approximated model

$$\min_{u,w} E(w, u) = \|w\|_p + \frac{\mu}{2} \|\Phi u - w\|_2^2 + \frac{\lambda}{2} \|\mathcal{P}_\Lambda(u - f)\|_2^2 \quad (5)$$

where μ is the positive penalizing factor. The approximated model is then solved by alternating minimization method as follows.

1) *Solving w* : Fixing u , the subproblem for w is

$$\min_w \|w\|_p + \frac{\mu}{2} \|w - \Phi u\|_2^2. \quad (6)$$

As is well known [38], in the case of $p = 0$, the subproblem (6) is solved by hard shrinkage, i.e.,

$$w = \max\{|\Phi u|, 1/\mu\} \text{sign}(\Phi u), \quad (7)$$

where sign function is defined as

$$\text{sign}(x) = \begin{cases} 1, & \text{if } x > 0, \\ 0, & \text{if } x = 0, \\ -1, & \text{if } x < 0. \end{cases}$$

In the case of $p = 1$ [31], problem (6) can be solved by soft shrinkage formula

$$w = \max\{|\Phi u| - 1/\mu, 0\} \text{sign}(\Phi u). \quad (8)$$

When $0 < p < 1$, there is no closed-form solution and we will not consider in this paper. In a whole, we use a uniform notation as

$$w = \text{shrink}_p(\Phi u, \tau),$$

where $\tau = 1/\mu$, $p = 0$ denotes hard shrinkage defined in (7) and $p = 1$ denotes soft shrinkage defined in (8).

Algorithm 1 ICI- Φ

- Initialization: $w^0 = \Phi(f)$, $u^0 = f$.
- For $k = 0, 1, 2, \dots$, repeat until maximum iteration is reached

$$w^{k+1} = \text{shrink}_p(\Phi u^k, \tau),$$

$$u^{k+1} = (\Phi^T \Phi + \gamma \mathcal{P}_\Lambda)^{-1} (\Phi^T w^{k+1} + \gamma \mathcal{P}_\Lambda f).$$

- Output: u^{k+1} .
-

2) *Solving u* : Fixing w , the subproblem for u is

$$\min_u \|\Phi u - w\|_2^2 + \gamma \|\mathcal{P}_\Lambda(u - f)\|_2^2 \quad (9)$$

where $\gamma = \lambda/\mu$. Assume that Φ^T is the conjugate operator of Φ . Then the Euler-Lagrange equation is

$$\Phi^T (\Phi u - w) + \gamma \mathcal{P}_\Lambda(u - f) = 0, \quad (10)$$

where we have used the simple fact that $\mathcal{P}_\Lambda^2 = \mathcal{P}_\Lambda$. Moreover, the close form solution for 9 is then given by

$$u = (\Phi^T \Phi + \gamma \mathcal{P}_\Lambda)^{-1} (\Phi^T w + \gamma \mathcal{P}_\Lambda f). \quad (11)$$

Finally, the algorithm is summarized in Algorithm 1 and is called iterative coupled inpainting (ICI).

Remark that when $\Phi = \nabla$, $p = 1$, model (1) is considered in [3], where gradient flow method is used in the numerical implementation. It is obvious that our numerical scheme is quite different. When Φ is tight frame, i.e., $\Phi^T \Phi = I$, the iteration of u^{k+1} can be simplified as

$$u^{k+1} = (I + \gamma \mathcal{P}_\Lambda)^{-1} (\Phi^T w^{k+1} + \gamma \mathcal{P}_\Lambda f).$$

Furthermore, if the hard constraint (2) is considered, the iteration formula of u becomes

$$u^{k+1} = \mathcal{P}_\Lambda f + (I - \mathcal{P}_\Lambda) \Phi^T w^{k+1}. \quad (12)$$

Plugging w^{k+1} into algorithm ICI- Φ in (12), we obtain the simplified iteration formula

$$u^{k+1} = \mathcal{P}_\Lambda f + (I - \mathcal{P}_\Lambda) \Phi^T \left(\text{shrink}_p(\Phi u^k, \tau) \right). \quad (13)$$

Note that this formulation is the same as the iteration scheme considered in [15], which is derived by other method. The convergence of iteration scheme (13) is also proved in [15].

C. Algorithm IDI

We remark that when Φ is gradient operator, wavelet or tight frame, it can be formulated as a fixed matrix. In particular, for wavelet and tight frame, the analysis matrix Φ and the synthesis matrix Φ^T satisfies

$$\Phi^T \Phi = I.$$

However, for the image adaptive denoising method such as dictionary learning [39]–[41] and BM3D filter [42], the analysis operator Φ is image adaptive, and Φ^T is not equal to the synthesis operator. In the following, we consider BM3D filter

Algorithm 2 IDI-BM3D

- Initialization: $w^0 = \Phi(f), u^0 = f$.
- For $k = 0, 1, 2, \dots$, repeat until maximum iteration is reached

$$\begin{aligned} w^{k+1} &= \text{shrink}_p(\Phi u^k, \tau), \\ u^{k+1} &= (I + \gamma \mathcal{P}_\Lambda)^{-1} (\Psi w^{k+1} + \gamma \mathcal{P}_\Lambda f). \end{aligned}$$

- Output: u^{k+1} .

as an example. Note that similar analysis holds for dictionary learning.

Assume that the analysis and synthesis operators of BM3D filter are Φ and Ψ respectively. The functions of Φ and Ψ are addressed as follows: When applying Φ on a 2D image x , we firstly collect similar image blocks in groups, then stack together the blocks in each group to form 3D data arrays, finally apply an invertible 3D transform \mathcal{T} on each 3D data array and get the 3D spectral data arrays $\omega (= \Phi x)$. Furthermore, when applying Ψ on a 3D spectral data arrays ω , we firstly invert each array of ω by inverse 3D transform \mathcal{T}^{-1} , then return the blocks of $\mathcal{T}^{-1}(\omega)$ to their original positions, finally the image is reconstructed as a weighted average of all blocks. In fact, Danielyan *et al.* [43] have derived the explicit formulation of Φ, Ψ . We will not recall the formulation in this paper in order to save pages since the formulation is long to write down. It is proved in [43] that Φ and Ψ have the following relationships

$$\Phi^T \Phi = \mathcal{W} > 0, \Psi = \mathcal{W}^{-1} \Phi^T, \Psi \Phi = I. \quad (14)$$

The entries of \mathcal{W} are defined by the data grouping and counting the number of times each pixel appears in different groups, such that the range can be very large. Then the matrix $\Phi^T \Phi + \gamma \mathcal{P}_\Lambda$ is ill conditioned and degrades the image restoration quality. To solve this problem, we replace Φ^T by Ψ in Algorithm 1 and get a new algorithm, which is called iterative decoupled inpainting BM3D (IDI-BM3D), see Algorithm 2. We remark that Φ and Ψ are image adaptive. Indeed, we denote $\Phi = \Phi(u^k)$ and $\Psi = \Psi(u^k)$ in Algorithm 2.

Let us give some interpretation of the main iteration steps in IDI-BM3D. When $\Psi = \Phi^T$, ICI is equivalent to IDI. However, it is not true when $\Psi \neq \Phi^T$. Different from the original iteration steps in Algorithm 1 which come from alternately minimizing the same functional $E(w, u)$, in IDI, w and u are minimizers of the following optimization with two decoupled functionals

$$\begin{cases} w = \arg \min_w \|w\|_p + \frac{\mu}{2} \|w - \Phi u\|_2^2, \\ u = \arg \min_u \|u - \Psi w\|_2^2 + \gamma \|\mathcal{P}_\Lambda(u - f)\|_2^2. \end{cases} \quad (15)$$

Here the w -problem is for denoising and the u -problem is for linear combination and projection.

The decoupling process has the advantage that various denoising methods can be applied in the first step and other projection methods can be used in the second step separately. In the denoising step, we can choose the over complete dictionary learning based denoising method and BM3D denoising method, which are the two state-of-the-art denoising methods.

In the second step, we can also consider the hard constraint (2) where the updating formula of u^{k+1} changes accordingly,

$$u^{k+1} = \mathcal{P}_\Lambda f + (I - \mathcal{P}_\Lambda) \Psi w^{k+1}. \quad (16)$$

We remark that the advantage of decoupling has also been shown in image deblurring and denoising methods [43], [44]. For example, the decoupled method IDD-BM3D [43] is currently the state-of-the-art deblurring method. In IDD-BM3D, the two iteration steps are decoupled as denoising and deblurring. BM3D filter is used in the denoising step.

III. CONVERGENCE ANALYSIS

We restrict $p = 1$ in this section. We mainly prove the convergence of ICI. Similar arguments hold for the convergence of IDI algorithm. When the penalty parameter $\mu \rightarrow +\infty$, according to the convergence of the quadratic penalty method [45, Th. 17.1], the solution of (5) converges to (1). But theoretically, it is hard to determine the best value of μ . In numerical application, we choose μ by tuning this parameter to achieve optimal result. In this section, we prove that the sequence $\{(w^k, u^k)\}$ generated by Algorithm 1 converges to a solution of problem (5).

Let us introduce some notations. Remark that the soft shrinkage defined in (8) is pointwise. Let us address it more clearly. For scalar $a \in \mathbb{R}$, the 1D soft shrinkage operator $s : \mathbb{R} \rightarrow \mathbb{R}$ is defined as

$$s(a) := \max\{|a| - \tau, 0\} \text{sign}(a). \quad (17)$$

For vector $a \in \mathbb{R}^n$, the soft shrinkage operator is then defined as

$$S(a) := (s(a_1); \dots; s(a_n)).$$

We also define a symmetric matrix

$$M := \Phi^T \Phi + \gamma \mathcal{P}_\Lambda.$$

With the notations, the iterations in Algorithm 1 can be rewritten as

$$\begin{cases} w^{k+1} = S(\Phi u^k), \\ u^{k+1} = M^{-1}(\Phi^T w^{k+1} + \gamma \mathcal{P}_\Lambda f). \end{cases} \quad (18)$$

Furthermore, by introducing a linear operator

$$h(w) := \Phi M^{-1}(\Phi^T w + \gamma \mathcal{P}_\Lambda f),$$

we can rewrite (18) in the following form

$$\begin{cases} w^{k+1} = S \circ h(w^k), \\ u^{k+1} = M^{-1}(\Phi^T w^{k+1} + \gamma \mathcal{P}_\Lambda f). \end{cases} \quad (19)$$

Firstly we prove that problem (5) has at least one solution. It is easy to show that the null space of \mathcal{P}_Λ is

$$\mathcal{N}(\mathcal{P}_\Lambda) = \{g \in R^N \mid g(x) = 0, \forall x \in \Lambda\}.$$

Assume that the following condition holds

$$\mathcal{N}(\Phi) \cap \mathcal{N}(\mathcal{P}_\Lambda) = \{0\}. \quad (20)$$

Remark that this condition holds for many popular transform in image processing. For example, when $\Phi = \nabla$ or $\Phi = W$

(wavelet transform, curvelet transform or other tight frame transform), we have

$$\mathcal{N}(\nabla) = \{c\mathbf{1}\} \text{ and } \mathcal{N}(\mathbf{W}) = \{\mathbf{0}\}$$

where c is an arbitrarily constant, such that condition (20) holds. Under condition (20), we can deduce that the functional $E(w, u)$ in (5) is coercive, i.e., $E(w, u)$ goes to infinity as $\|(w, u)\| \rightarrow \infty$. Moreover, $E(w, u)$ is convex and bounded from below. Therefore, by standard argument in [46], we conclude that $E(w, u)$ has at least one minimizer pair (w^*, u^*) which satisfies the Euler-Lagrange equations, or equivalently

$$\begin{cases} w^* = S \circ h(w^*), \\ u^* = M^{-1}(\Phi^T w^* + \gamma \mathcal{P}_\Lambda f). \end{cases} \quad (21)$$

The first equation of (21) means that w^* is a fixed point of $S \circ h$. Then the convergence analysis can be established based on the properties of non-expansive operators S and h .

Remark that the non-expansiveness of 2D soft shrinkage operator is proved in [47, Proposition 3.1]. The proof of 1D case is not addressed in the literature to the best of our knowledge, so we give a direct proof.

Proposition 1: For any $a, b \in \mathbb{R}$, we have

$$|s(a) - s(b)| \leq |a - b|$$

and the equality holds if and only if $s(a) - s(b) = a - b$.

See appendix A for the proof of Proposition 1.

It follows directly from Proposition 1 that S is a non-expansive operator. We can also prove the non-expansiveness of operator h .

Proposition 2: For any w, \tilde{w} in the range of Φ , we have

$$\|h(w) - h(\tilde{w})\| \leq \|w - \tilde{w}\| \quad (22)$$

and the equality holds if and only if $h(w) - h(\tilde{w}) = w - \tilde{w}$.

See appendix B for the proof of Proposition 2.

Based on Proposition 1 and Proposition 2, we are ready to prove the convergence of ICI in the following theorem.

Theorem 1: Assume that condition (20) holds. Then for any fixed $\tau > 0, \gamma > 0$, the sequence $\{(w^k, u^k)\}$ generated by ICI- Φ converges to a solution (w^*, u^*) of problem (5).

See appendix C for the proof of Theorem 1.

With similar arguments as in the proof of ICI, we can prove the following convergence result for IDI when Φ is chosen as BM3D frame.

Theorem 2: Assume that the fix point set of problem (15) is nonempty. Then for any fixed $\tau > 0, \gamma > 0$, the sequence $\{(w^k, u^k)\}$ generated by IDI-BM3D converges to a fixed point (w^*, u^*) of problem (15).

See appendix D for the proof of Theorem 2.

IV. EXPERIMENTS AND COMPARISONS

In this section, we apply the proposed algorithm on a variety of natural images. The application includes the following image inpainting problems: text and scratch removal, randomly missing pixels filling, and small size missing block completion. In these examples, we compare the effects of different regularization operator Φ in our framework and we

also compare our method with some of the existing pixel-based and patch-based inpainting methods. These methods include cubic interpolation based on Delaunay triangulation (implemented by MATLAB routine “griddata”), sparsity based methods ECM [19] and MCA [18] (the source codes MCAlab can be downloaded from web page¹), exemplar based method (EBM for short) in [24], coherence transport method [13] (CTM for short, see the source codes on webpage²) and smooth ordering patches based method SOP [21]. All the key parameters are tuned carefully in each method and the optimal result is chosen to compare.

The default parameters of the proposed methods are $\gamma = 1000, \tau = \sigma$ is the estimation of noise standard device, patch size of IDI-BM3D is 8, 16 or 32. We choose the patch size which is most close to the width of inpainting mask. The stopping criterion of the proposed algorithms is that the user defined maximum iteration is attained. The maximum iteration is set by trail and error. Remark that to speed up the algorithm, firstly, we choose the cubic interpolation result as initialization of IDI-BM3D. Secondly, since larger σ corresponds to faster diffusion speed and smaller σ corresponds to higher inpainting quality (which will be addressed in section IV.D), we choose to decrease the noise estimate σ from 15, 10, 5 to 2 during iteration and for each σ we perform the same number of iterations.

All the experiments are performed under Windows 7 and MATLAB R2012a with Intel Core i7-3840QM CPU@2.80GHz and 8GB memory. The programming language is mixed MATLAB and C.

A. Text and Scratch Removal

In Figs. 1-3, we apply the proposed algorithm with different regularization operator Φ on text and scratch removal of a gray scale image. Typically, we choose Φ as gradient operator, wavelet transform, framelet transform and BM3D transform. When $\Phi = \nabla, A = \nabla^T \nabla + \gamma \mathcal{P}_\Lambda$ is a large sparse matrix and backslash operator in MATLAB is used to solve u . For BM3D transform, we use decoupled algorithm IDI-BM3D.

In Fig. 1, the test image Fig. 1(a) is a piecewise smooth image with simple geometric structures. The white texts in Fig. 1(b) denote the missing region. Fig. 1(c)-(f) are the inpainting results of TV, wavelet, framelet and BM3D regularization respectively. Visually, the result of ICI-wavelet (Fig. 1(d)) has some artifacts and has the lowest PSNR. The result of ICI-TV is slightly better than ICI-wavelet. ICI-framelet gains better visual quality and higher PSNR value than ICI-TV and ICI-wavelet. The result of IDI-BM3D is the best which gains PSNR about 9dB higher than others. It is obvious that TV, wavelet and framelet all fail to recover the horizontal line in the bottom part since it is broken in Fig 1(c)-(e). In contrast, IDI-BM3D can recover this line perfectly in Fig. 1(f).

In Fig. 2, we test the Barbara image with many textures. Fig. 2(a) is the original Barbara image. The white scratches in Fig. 2(b) denote the information missing region. Comparing

¹<https://fadili.users.greyc.fr/demos/WaveRestore/downloads/mcalab/Home.html>

²<https://github.com/maerztom/inpaintBCT>

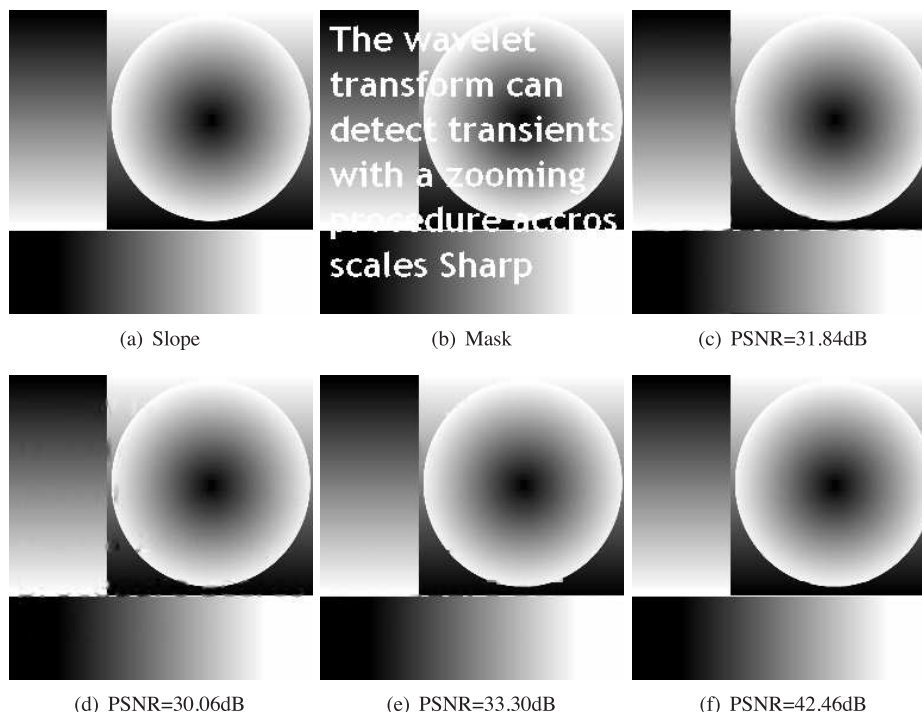


Fig. 1. Text removal by the proposed method with different regularization operator Φ . (a) The original image; (b) image with white words as inpainting mask; (c) result of ICI-TV, iteration = 1000, time = 129s; (d) result of ICI-Wavelet, iteration = 600, time = 17s; (e) result of ICI-Framelet, iteration = 600, time = 19s; (f) result of IDI-BM3D, patch size = 8, iteration = 200, time = 133s.

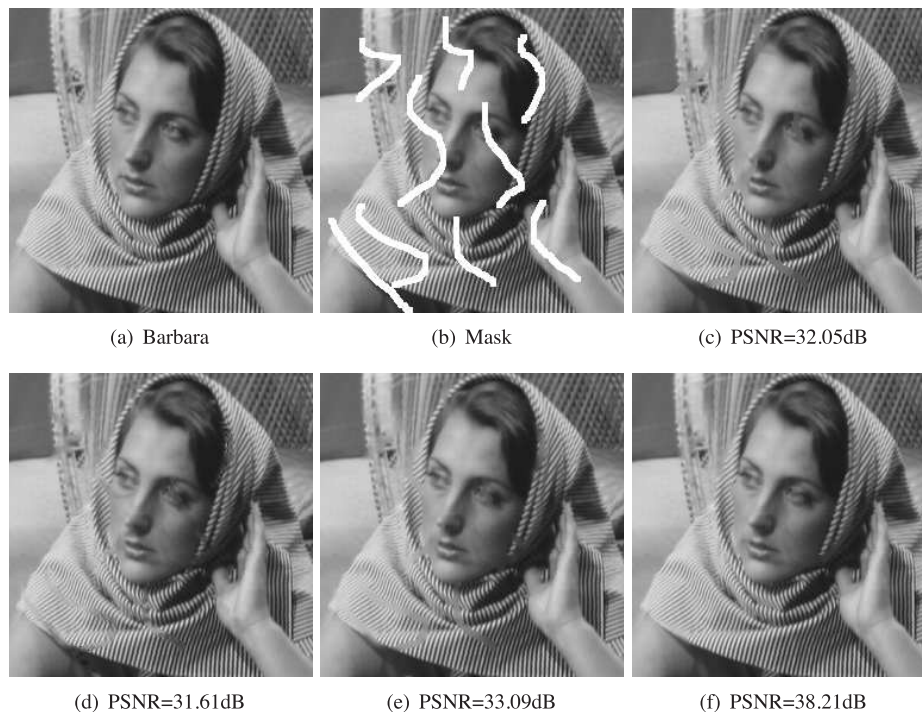


Fig. 2. Scratch removal by the proposed method with different regularization operator Φ . (a) The original image; (b) image with white scratches as inpainting mask; (c) result of ICI-TV, iteration = 1000, time = 134s; (d) result of ICI-Wavelet, iteration = 600, time = 20s; (e) result of ICI-Framelet, iteration = 600, time = 48s; (f) result of IDI-BM3D, patch size = 8, iteration = 200, time = 127s.

Fig. 2(c)-(f), we find that our method IDI-BM3D can recover most of the textures and has much higher PSNR than the others (more than 5dB). However, in Fig. 2(c)-(e) the missing region is filled by smooth information which implies that the

textures can not propagate into the missing region by these methods.

In Fig. 3, IDI-BM3D method achieves higher PSNR values than other three methods about at least one dB.

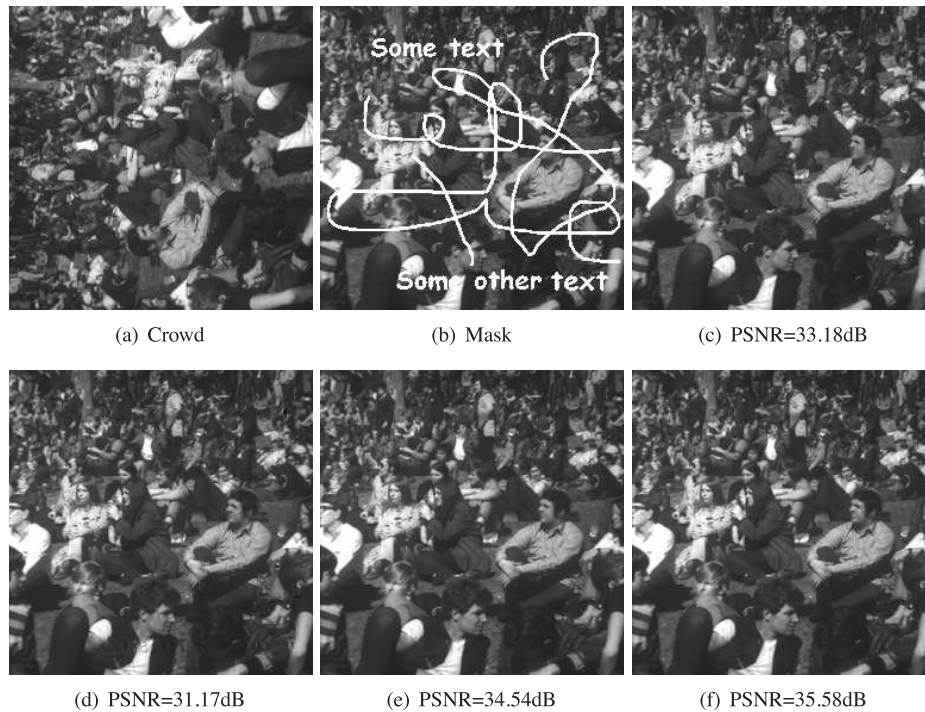


Fig. 3. Scratch and text removal by the proposed method with different regularization operator Φ . (a) The original image; (b) image with white words and scratches as inpainting mask; (c) result of ICI-TV, iteration = 1000, time = 140s; (d) result of ICI-Wavelet, iteration = 600, time = 16s; (e) result of ICI-Framelet, iteration = 600, time = 53s; (f) result of IDI-BM3D, patch size = 8, iteration = 200, time = 118s.

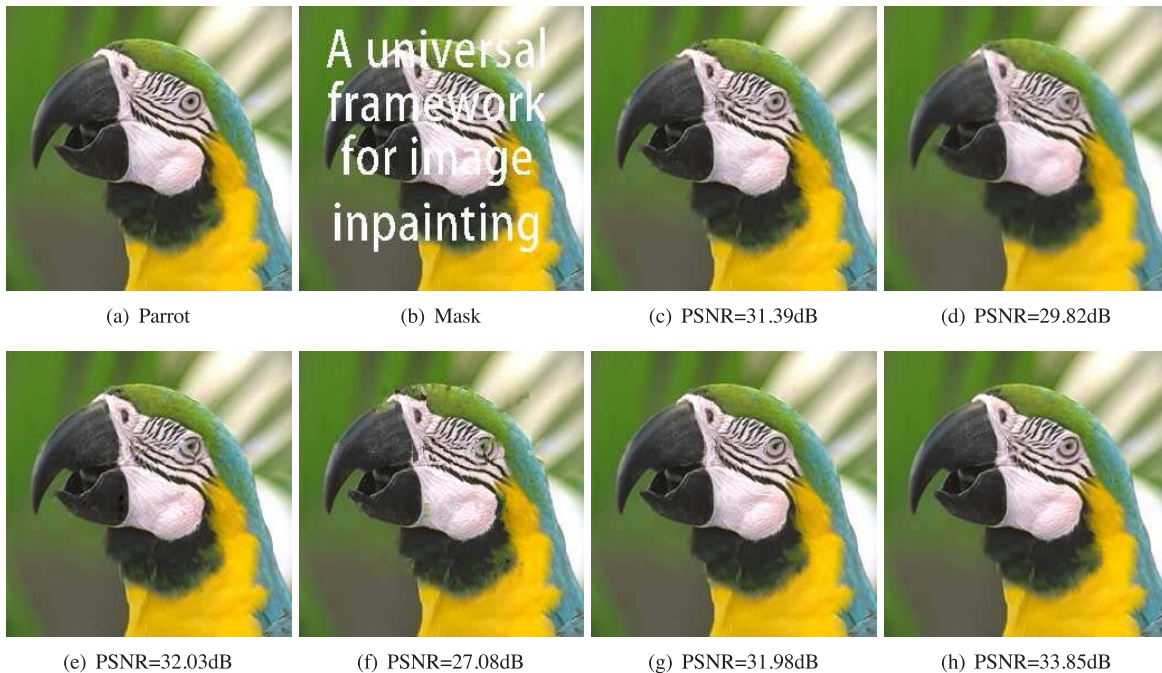


Fig. 4. Text removal by different inpainting methods. (a) The original image; (b) image with inpainting mask marked by white words; (c) result of cubic interpolation, time = 1.3s; (d) result of ECM [19], time = 157s; (e) result of MCA [18], time = 554s; (f) result of EBM [24], time = 164s; (g) result of CTM [13], time = 0.1s; (h) result of our method IDI-BM3D, patch size = 8, iteration = 200, time = 217s.

Some difference of the inpainting results can be seen by zooming in. However, visually the improvement is not very prominent.

We remark that in the test images of Figs. 1-2, there are many similar structures existing in the same image.

For instance, the patterns are quite similar along the horizontal line in Fig. 1(a) and that on Barbara's scarf in Fig. 2(a). While in the Crowd image in Fig. 3(a), there are fewer similar structures. From the results in Fig. 1-3, we can conclude that IDI-BM3D works much better than

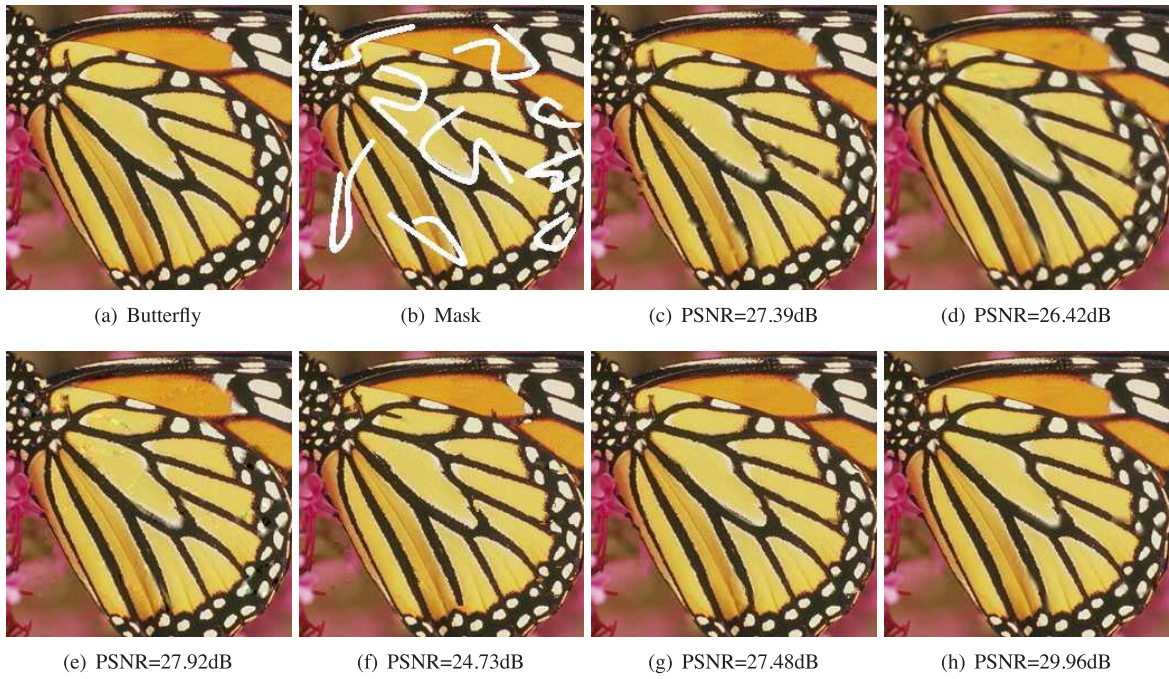


Fig. 5. Scratch removal by different inpainting methods. (a) The original image; (b) image with white scratches as inpainting mask; (c) result of cubic interpolation, time = 1.3s; (d) result of ECM [19], time = 206s; (e) result of MCA [18], time = 539s; (f) result of EBM [24], time = 119s; (g) result of CTM [13], time = 0.1s; (h) result of our method IDI-BM3D, patch size = 8, iteration = 200, time = 183s.

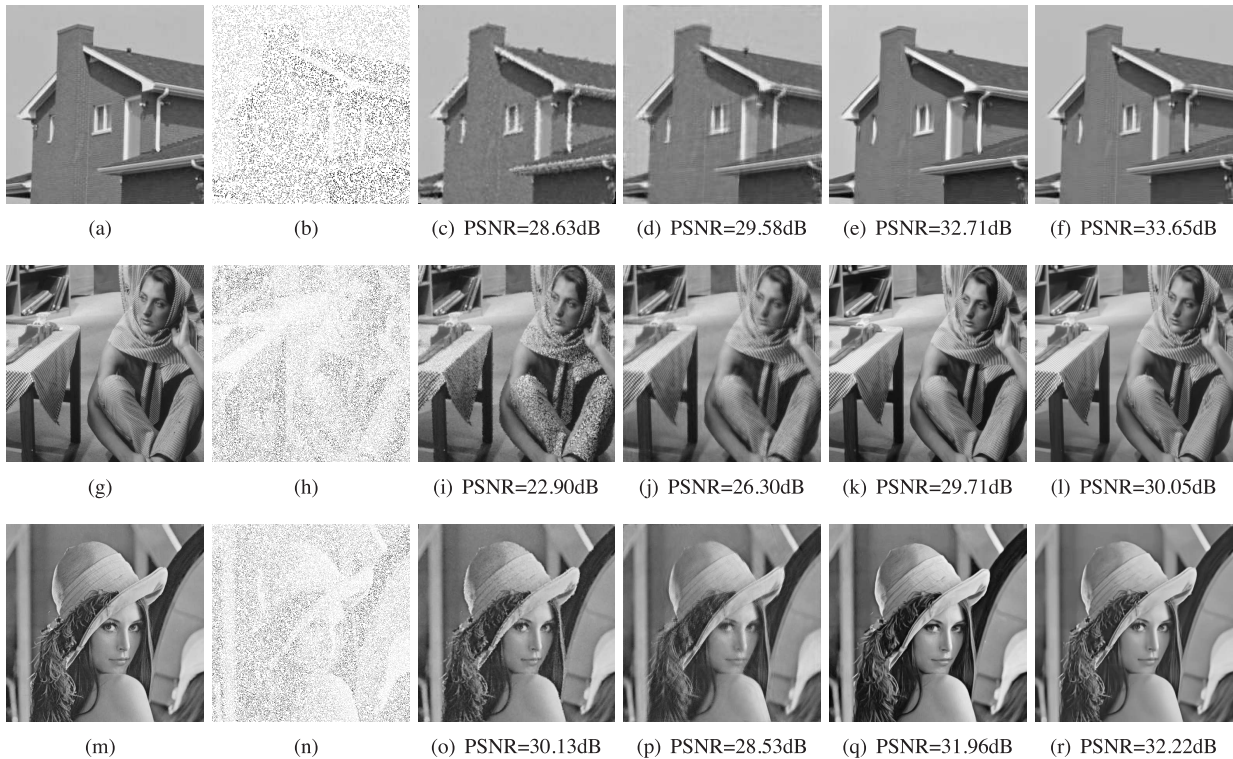


Fig. 6. Inpainting results of corrupted versions of images House, Barbara, and Lena with randomly 80% of their pixels missing, obtained with different reconstruction methods: First column - original image, Second column - corrupted images, Third column - Cubic interpolation, Fourth column - MCA [18], Fifth column - SOP [21], Sixth column - Ours.

other methods when the image contains many similar patches, while for image with fewer similar patches, the advantage of IDI-BM3D will not be so prominent. The underline reason is that IDI-BM3D method is based on patch similarity as BM3D.

If the missing patches exist outside the inpainting region, they can mostly be recovered by IDI-BM3D. However, if no similar patch is available, it is hard to recover the missing region.

The experiments in Figs. 1-3 show that IDI-BM3D method achieves the best result in the four types of transform operator Φ . So in the following experiments, we choose IDI-BM3D as our representative method and compare it with other methods.

In Fig. 4 and Fig. 5, we test text and scratch removal of color images, and compare our method with some pixel based methods and exemplar based method which include cubic interpolation, ECM, MCA, EBM and CTM. Fig. 4(a) and Fig. 5(a) show the original Parrot and Butterfly images. The white text and scratches in Fig. 4(b) and Fig. 5(b) denote the missing regions. Cubic interpolation gives good results which have higher PSNR values than ECM and EBM. However, in the results of cubic interpolation, there are many artifacts along edges, for example, along the edges of the parrot's beak and the black line patterns of the butterfly. We note that EBM works well for large size object removal. But for small size inpainting region, the results in Fig. 4(f) and Fig. 5(f) seem not good which have the lowest PSNR among all. The results of MCA also have some color artifacts which is very obvious in Fig. 5(e). The results of CTM in Fig. 4(g) and Fig. 5(g) seem plausible. However, by careful observation, we can see some unsatisfactory artifacts. Among all, our method gives the best results both in visual aspect and in terms of PSNR.

B. Randomly Missing Pixels Filling

In this test, we demonstrate the performance of our proposed method on randomly missing pixels filling. We compare our results with cubic interpolation, MCA and SOP. The original images include House, Barbara and Lena as displayed in the first column of Fig. 6. The second column of Fig. 6 show the corrupted images obtained by randomly choosing 80% of their pixels missing. The missing pixels are displayed in white color. The third column show the results of cubic interpolation. There are many artifacts along the edges of the house and on the texture part of Barbara. MCA blurs the images while inpainting, see the fourth column. The results of SOP and our method have the best visual quality. In terms of PSNR, our method is about 0.5dB (in average) higher than SOP.

C. Missing Block Completion

In this test, we consider relative larger size region inpainting. We extract a subregion from Barbara and House as original images, see Fig. 7(a) and Fig. 8(a). The inpainting mask is a white block with size 32×32 as shown in Fig. 7(b) and Fig. 8(b). The results of cubic interpolation in Fig. 7(c) and Fig. 8(c) seem not good for this large inpainting region. ECM oversmooths the textures on Barbara in Fig. 7(d) and can not recover the eave in Fig. 8(d). CTM gives somewhat strange results in Fig. 7(g) and Fig. 8(g). MCA, EBM and our method provide better results than the others. Among all, our method has best visual quality and PSNR values. Let us compare these three methods in Fig. 7. MCA can not recover most of the textures on Barbara and brings some artifacts in Fig. 7(e). EBM can recover the textures but bring also artifacts. Our method can recover most of the textures with some oversmoothness along edge. In a whole, our method has

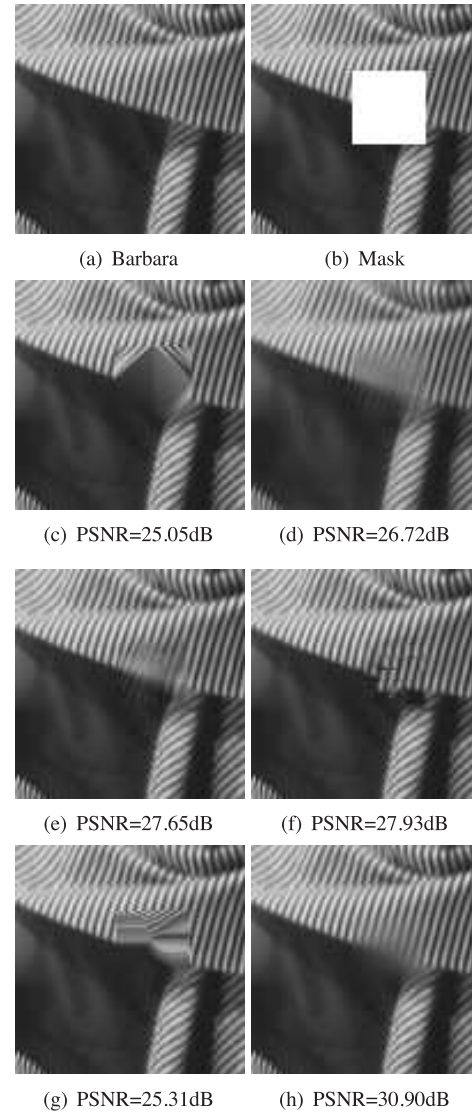


Fig. 7. Block completion. (a) The original image; (b) image with white block mask, size 32×32 ; (c) result of cubic interpolation; (d) result of ECM [19]; (e) result of MCA [18]; (f) result of EBM [24]; (g) result of CTM [13]; (h) result of our method IDI-BM3D.

PSNR of roughly 3dB higher than the second best. For House image, MCA, EBM and our method can recover the eave. But some of the lightness are lost in Fig. 8(e). EBM and our method provide visually perfect results. In terms of PSNR, our method is about 1dB higher than EBM.

D. Computational Time and Effect of Parameters

To display the computational efficiency of the proposed algorithm, we report the computational time of each method in Figs. 1-5. For 256×256 gray image and color image, IDI-BM3D takes about 0.6 and 1 second to perform one iteration. As a whole, IDI-BM3D achieves the best results at about 200 iterations in Fig. 1-5 among all compared methods. From Figs. 1-3, we find that ICI-wavelet and ICI-framelet are much faster than ICI-TV and IDI-BM3D. The total computational time of ICI-TV and IDI-BM3D are similar. Fig. 4 and Fig. 5 tell us that CTM is the fastest one among all which

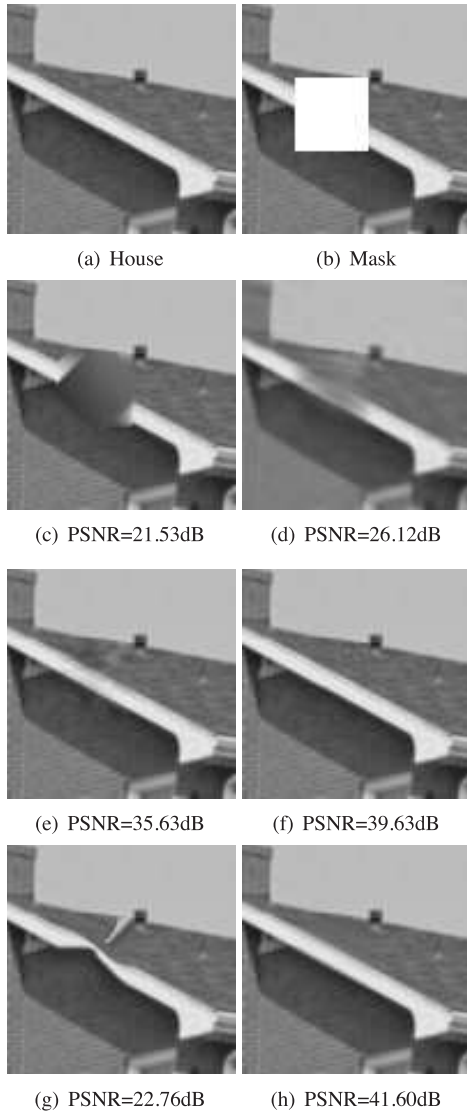


Fig. 8. Block completion. (a) The original image; (b) image with white block mask, size 32×32 ; (c) result of cubic interpolation; (d) result of ECM [19]; (e) result of MCA [18]; (f) result of EBM [24]; (g) result of CTM [13]; (h) result of our method IDI-BM3D.

takes only 0.1 second. Cubic interpolation is the second fast which takes 1.3 seconds. The other methods include ECM, MCA EBM and our IDI-BM3D consume several hundreds of seconds. Among all, MCA is the most computational expensive. Remark that we use the default stopping criterion of ECM and MCA in the original codes.

There are mainly two parameters in our model, namely, γ and τ . Remark that the parameter τ is set as the noise standard deviation estimation σ in the denoising step. When IDI-BM3D is used, there is another important parameter, patch size. Based on the experiments, we find that our method is not sensitive to γ if it is large enough. The reason is when $\gamma = \frac{\lambda}{\mu}$ is sufficiently large, the projection term will be dominating in the u subproblem in (5). Therefore, u almost equals f outside the inpainting region. Inside the inpainting region, $\gamma = 0$, so the projection term has no effect. In all the experiments, γ is set to be 1000. Remark that the range of image is $[0,255]$. Patch size and τ are very important

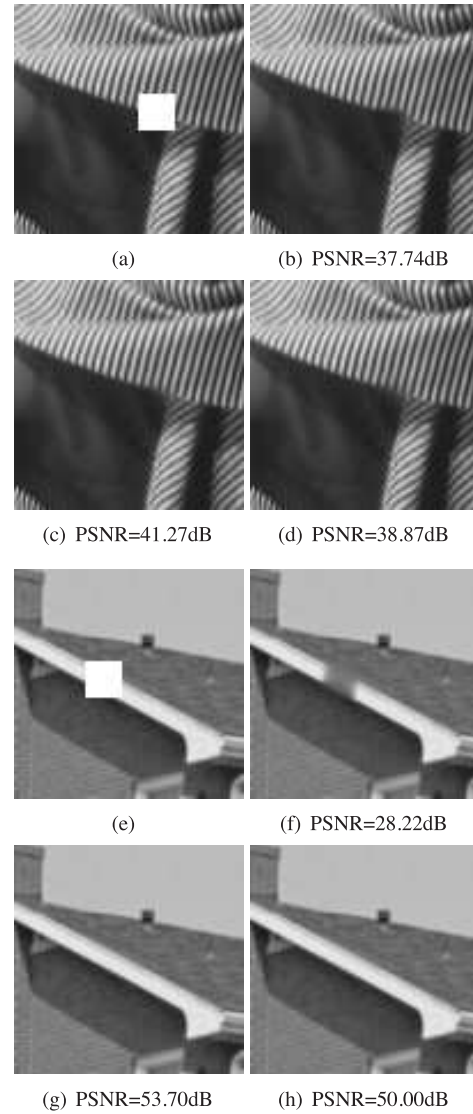


Fig. 9. Block completion with different patch size in our method IDI-BM3D. First column - image with mask, block size 16×16 ; Second column to Fourth column - our results with patch size = 8, 16 and 32 respectively.

parameters which affect both the computational time and the image quality.

To illustrate the influence of patch size, in Fig. 9, we test 16×16 size block completion with different patch size in IDI-BM3D. The results show that when the patch size is close to the missing block, the results gain best visual quality and PSNR. When the patch size is smaller than the block size, the eave can not be connected in the House image.

The influence of parameter $\tau = \sigma$ on the proposed method IDI-BM3D is demonstrated in Fig. 10. We set $\sigma = [5, 10, 15, 20, 25, 30, 35, 40, 45, 50]$ and apply our method on Fig. 9(e). The PSNR and computation time as functions of σ are displayed in Fig. 10(a)-(b). We can see that PSNR is decreasing with σ , however, the computational time is increasing with σ . That means, high quality image needs more computational time. We should note that in our experiments we do the iterations on the whole image, narrow band method may be used to largely alleviate the computation burden. When narrow band method is used, we can calculate only

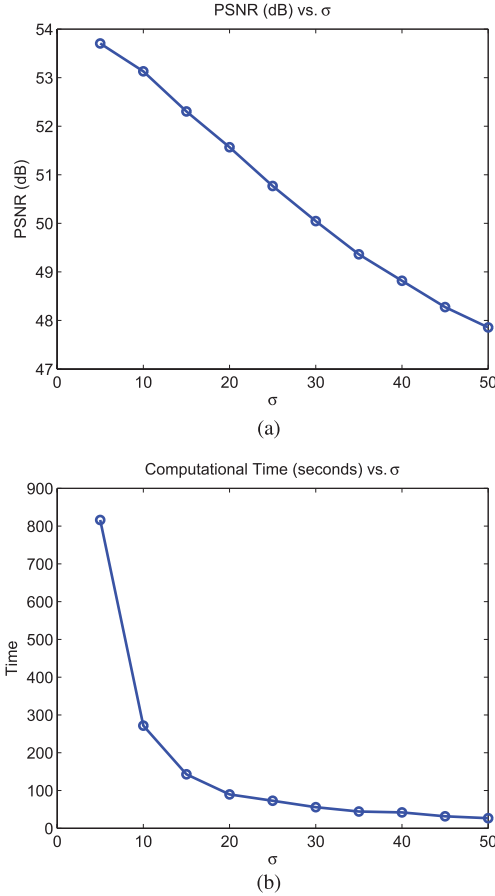


Fig. 10. The effect of parameters in our method IDI-BM3D. (a) PSNR vs. σ ; (b) Computational time vs. σ .

on narrow band around the inpainting mask and inside the inpainting region. This will be our future work.

V. CONCLUSION

This paper proposed a universal variational framework for image inpainting. The major novelty of this paper is the construction of the universal algorithm framework ICI, IDI and the convergence analysis. In the ICI framework, many existing regularization operator can be used. For patch based regularization operator such as BM3D transform and dictionary learning, IDI is more suitable than ICI. Experiments and comparisons showed that the proposed IDI-BM3D can produce state of the art results in inpainting problems include text and scratch removal, randomly missing pixels filling and block completion.

In the future work, firstly, since for images with fewer similar structures, the advantage of IDI-BM3D is not so prominent, we will do our effort to enhance the inpainting quality of this kind of images. One possible way is learning some patches from other images with the desired structures. Secondly, we will generalize our framework to other image processing problems such as image deblurring and image segmentation. With the idea of decoupling, we can utilize the most efficient regularization schemes such that it is very possible to enhance the recovered image quality and segmentation accuracy.

APPENDIX A

PROOF OF PROPOSITION 1

Let us separate \mathbb{R} into three disjoint subsets $E_1 = (-\infty, -\tau)$, $E_2 = [-\tau, \tau]$, $E_3 = (\tau, +\infty)$ where $\tau > 0$. Without loss of generality, we assume $a \geq b$. Then there are the following six cases:

- (i) $a, b \in E_1, s(a) - s(b) = (a + \tau) - (b + \tau) = a - b$;
- (ii) $a \in E_2, b \in E_1, |s(a) - s(b)| = |0 - (b + \tau)| = -b - \tau < a - b = |a - b|$;
- (iii) $a \in E_3, b \in E_1, |s(a) - s(b)| = |(a - \tau) - (b + \tau)| = a - b - 2\tau < |a - b|$;
- (iv) $a \in E_2, b \in E_2, s(a) - s(b) = 0 - 0 = 0$;
- (v) $a \in E_3, b \in E_2, |s(a) - s(b)| = |a - \tau - 0| = a - \tau < a - b = |a - b|$;
- (vi) $a, b \in E_3, s(a) - s(b) = (a - \tau) - (b - \tau) = a - b$.

In all the cases, we have $|s(a) - s(b)| \leq |a - b|$. The equality can be hold in case (i)(iv)(vi), in which it obviously holds that $s(a) - s(b) = a - b$.

APPENDIX B

PROOF OF PROPOSITION 2

Proof: Denote the symmetric matrix $T = \Phi M^{-1} \Phi^T$. We first claim that the eigenvalues of T , denote as $\rho(T)$, satisfy $0 \leq \rho(T) \leq 1$. As $\mathcal{N}(\Phi) \cap \mathcal{N}(\mathcal{P}_\Lambda) = \{0\}$ in assumption (20), M is positive definite and then M^{-1} is also positive definite. Hence T is obviously semi-positive definite with $\rho(T) \geq 0$ since

$$T = \Phi M^{-\frac{1}{2}} M^{-\frac{1}{2}} \Phi^T = B^T B,$$

where $B = M^{-\frac{1}{2}} \Phi^T$. Meanwhile, by [48, Th. 1.3.20], $T = \Phi M^{-1} \Phi^T$ have the same eigenvalues as

$$M^{-1} \Phi^T \Phi = M^{-1} (M - \gamma \mathcal{P}_\Lambda) = I - \gamma M^{-1} \mathcal{P}_\Lambda.$$

As $M^{-1} \mathcal{P}_\Lambda$ and $M^{-\frac{1}{2}} \mathcal{P}_\Lambda M^{\frac{1}{2}}$ are congruent matrices, their eigenvalues have the same symbols. Moreover, since $M^{-\frac{1}{2}} \mathcal{P}_\Lambda M^{\frac{1}{2}}$ is similar to \mathcal{P}_Λ , they have the same eigenvalues. Using the fact that $\lambda(\mathcal{P}_\Lambda) \geq 0$, we can conclude that $\lambda(M^{-1} \mathcal{P}_\Lambda) \geq 0$ and thus $\rho(T) \leq 1$.

By the definition of h , we have

$$\begin{aligned} \|h(w) - h(\tilde{w})\| &= \|\Phi M^{-1} (\Phi^T w + \gamma \mathcal{P}_\Lambda f) - \Phi M^{-1} (\Phi^T \tilde{w} + \gamma \mathcal{P}_\Lambda f)\| \\ &= \|T(w - \tilde{w})\| \leq \max |\rho(T)| \|w - \tilde{w}\| \leq \|w - \tilde{w}\|. \end{aligned}$$

Let $T = U^T \Lambda U$ be the eigen-decomposition of T , where U is an orthogonal matrix and Λ is a diagonal matrix with elements in $[0, 1]$. If the equality holds, we have $\|U^T \Lambda U(w - \tilde{w})\| = \|w - \tilde{w}\|$, and then $\|\Lambda U(w - \tilde{w})\| = \|U(w - \tilde{w})\|$. Since Λ is diagonal with nonnegative elements in $[0, 1]$, we deduce that $\Lambda U(w - \tilde{w}) = U(w - \tilde{w})$. Multiplying both sides by U^T , we get $h(w) - h(\tilde{w}) = w - \tilde{w}$.

APPENDIX C

PROOF OF THEOREM 1

Proof: The non-expansiveness of operators S and h implies that $\{w^k\}$ is bounded sequence, and hence there exists a subsequence w^{k_j} and a limit point w^* , such that $w^* = \lim_{j \rightarrow \infty} w^{k_j}$.

Let \hat{w} be any fixed point of $S \circ h$, namely, $\hat{w} = S \circ h(\hat{w})$. Using the non-expansiveness of S and h , we get

$$\|w^k - \hat{w}\| = \|S \circ h(w^{k-1}) - S \circ h(\hat{w})\| \leq \|w^{k-1} - \hat{w}\|.$$

Hence $\|w^k - \hat{w}\|$ is monotonically decreasing, and the limit exists

$$\lim_{k \rightarrow \infty} \|w^k - \hat{w}\| = \lim_{j \rightarrow \infty} \|w^{kj} - \hat{w}\| = \|w^* - \hat{w}\|. \quad (23)$$

This means that all the limit points of $\{w^k\}$ have equal distance to \hat{w} . By continuity of $S \circ h$, we get

$$S \circ h(w^*) = \lim_{j \rightarrow \infty} S \circ h(w^{kj}) = \lim_{j \rightarrow \infty} w^{kj+1}.$$

So $S \circ h(w^*)$ is also a limit point of the sequence $\{w^k\}$, and then

$$\|w^* - \hat{w}\| = \|S \circ h(w^*) - \hat{w}\| = \|S \circ h(w^*) - S \circ h(\hat{w})\|.$$

From Proposition 1 and Proposition 2, we know that the above equality holds if and only if

$$w^* - \hat{w} = h(w^*) - h(\hat{w}) = S \circ h(w^*) - S \circ h(\hat{w})$$

Therefore, we get $w^* = S \circ h(w^*)$, which means w^* is also a fixed point of $S \circ h$. Then we can replace \hat{w} in (24) by w^* , and get

$$\lim_{k \rightarrow \infty} \|w^k - w^*\| = \lim_{j \rightarrow \infty} \|w^{kj} - w^*\| = \|w^* - w^*\| = 0. \quad (24)$$

It implies the convergence of sequence w^k , i.e.,

$$\lim_{k \rightarrow \infty} w^k = w^*.$$

From the second iteration formula in (19), the convergence of u^k follows immediately, i.e.,

$$\begin{aligned} \lim_{k \rightarrow \infty} u^k &= \lim_{k \rightarrow \infty} M^{-1}(\Phi^T w^k + \gamma \mathcal{P}_\Lambda f) \\ &= M^{-1}(\Phi^T w^* + \gamma \mathcal{P}_\Lambda f) \\ &= u^*. \end{aligned}$$

Therefore, (u^*, w^*) satisfies (21), which means that it is a minimizer pair of (5).

APPENDIX D PROOF OF THEOREM 2

Proof: Replacing Φ^T by BM3D synthesis operator $\Psi(u^k)$ in all the arguments in the proof of Proposition 2 and Theorem 1, we find that the key point we need to prove is the non-expansiveness of operator h defined as

$$h(w) = \Phi(u^k)M^{-1}(\Psi(u^k)w + \gamma \mathcal{P}_\Lambda f), \quad (25)$$

where $M = I + \gamma \mathcal{P}_\Lambda$, $\Psi(u^k) = \mathcal{W}^{-1}(u^k)\Phi^T(u^k)$. Note that $\mathcal{W}(u^k)$ is a diagonal matrix with positive diagonal elements [43] $w_i > 0$. Let $T = \Phi M^{-1}\Psi$, we claim that the spectral radius of T satisfies $\rho(T) \leq 1$. To prove this claim, we assume the singular value decomposition of Φ is $\Phi = U\Sigma V^T$ that U and V are orthogonal matrices, Σ is diagonal matrix with nonnegative elements $\sigma_i \geq 0$. Then $\Phi^T\Phi = V\Sigma^T\Sigma V^T$.

By (14), $\Phi^T\Phi = \mathcal{W} > 0$. We deduce that $\sigma_i^2 = w_i > 0$. It is easy to derive that

$$\begin{aligned} T &= U\Sigma V^T(I + \gamma \mathcal{P}_\Lambda)^{-1}\mathcal{W}^{-1}V\Sigma^T U^T \\ &= U\Sigma\Sigma^T(I + \gamma \mathcal{P}_\Lambda)^{-1}\mathcal{W}^{-1}U^T. \end{aligned}$$

Then the i th eigenvalue of T is equal to 1 or $\frac{w_i}{(1+\gamma)w_i} \leq 1$, that is, $\rho(T) \leq 1$.

Therefore, the proof of Proposition 2 holds when Φ , Φ^T are replaced by $\Phi(u^k)$ and $\Psi(u^k)$, and such that Proposition 2 holds for operator h defined in (25). Following a similar deduction as in the proof of Theorem 1, we can prove Theorem 2 which is omitted.

ACKNOWLEDGMENT

The authors would like to thank Elad, Fadili and März for their source codes of MCA, ECM and CTM methods for comparisons. We would like to thank all the anonymous referees for their useful comments and suggestions.

REFERENCES

- [1] M. Bertalmio, G. Sapiro, V. Caselles, and C. Ballester, "Image inpainting," in *Proc. 27th Annu. Conf. Comput. Graph. Interact. Techn.*, 2000, pp. 417–424.
- [2] C. Ballester, M. Bertalmio, V. Caselles, G. Sapiro, and J. Verdera, "Filling-in by joint interpolation of vector fields and gray levels," *IEEE Trans. Image Process.*, vol. 10, no. 8, pp. 1200–1211, Aug. 2001.
- [3] J. Shen and T. F. Chan, "Mathematical models for local nontexture inpainting," *SIAM J. Appl. Math.*, vol. 62, no. 3, pp. 1019–1043, 2002.
- [4] S. Masnou and J.-M. Morel, "Level lines based disocclusion," in *Proc. Int. Conf. Image Process. (ICIP)*, Oct. 1998, pp. 259–263.
- [5] J. Shen, S. H. Kang, and T. F. Chan, "Euler's elastica and curvature-based inpainting," *SIAM J. Appl. Math.*, vol. 63, no. 2, pp. 564–592, 2003.
- [6] H. Grossauer and O. Scherzer, "Using the complex Ginzburg–Landau equation for digital inpainting in 2D and 3D," in *Scale Space Methods in Computer Vision*. New York, NY, USA: Springer-Verlag, 2003, pp. 225–236.
- [7] A. L. Bertozzi, S. Esedoglu, and A. Gillette, "Inpainting of binary images using the Cahn–Hilliard equation," *IEEE Trans. Image Process.*, vol. 16, no. 1, pp. 285–291, Jan. 2007.
- [8] M. Burger, L. He, and C.-B. Schönlieb, "Cahn–Hilliard inpainting and a generalization for grayvalue images," *SIAM J. Imag. Sci.*, vol. 2, no. 4, pp. 1129–1167, 2009.
- [9] X.-C. Tai, S. Osher, and R. Holm, "Image inpainting using a TV-stokes equation," in *Image Processing Based on Partial Differential Equations*. New York, NY, USA: Springer-Verlag, 2007, pp. 3–22.
- [10] F. Li, Z. Bao, R. Liu, and G. Zhang, "Fast image inpainting and colorization by Chambolle's dual method," *J. Vis. Commun. Image Represent.*, vol. 22, no. 6, pp. 529–542, 2011.
- [11] X.-C. Tai, J. Hahn, and G. J. Chung, "A fast algorithm for Euler's elastica model using augmented Lagrangian method," *SIAM J. Imag. Sci.*, vol. 4, no. 1, pp. 313–344, 2011.
- [12] F. Bornemann and T. März, "Fast image inpainting based on coherence transport," *J. Math. Imag. Vis.*, vol. 28, no. 3, pp. 259–278, 2007.
- [13] T. März, "Image inpainting based on coherence transport with adapted distance functions," *SIAM J. Imag. Sci.*, vol. 4, no. 4, pp. 981–1000, 2011.
- [14] M. K. Ng, X. Yuan, and W. Zhang, "Coupled variational image decomposition and restoration model for blurred cartoon-plus-texture images with missing pixels," *IEEE Trans. Image Process.*, vol. 22, no. 6, pp. 2233–2246, Jun. 2013.
- [15] J.-F. Cai, R. H. Chan, and Z. Shen, "A framelet-based image inpainting algorithm," *Appl. Comput. Harmon. Anal.*, vol. 24, no. 2, pp. 131–149, Mar. 2008.
- [16] R. H. Chan, S. Setzer, and G. Steidl, "Inpainting by flexible haar-wavelet shrinkage," *SIAM J. Imag. Sci.*, vol. 1, no. 3, pp. 273–293, 2008.
- [17] O. G. Guleryuz, "Nonlinear approximation based image recovery using adaptive sparse reconstructions and iterated denoising—Part II: Adaptive algorithms," *IEEE Trans. Image Process.*, vol. 15, no. 3, pp. 555–571, Mar. 2006.

- [18] M. Elad, J.-L. Starck, P. Querre, and D. L. Donoho, "Simultaneous cartoon and texture image inpainting using morphological component analysis (MCA)," *Appl. Comput. Harmon. Anal.*, vol. 19, no. 3, pp. 340–358, Nov. 2005.
- [19] M.-J. Fadili, J.-L. Starck, and F. Murtagh, "Inpainting and zooming using sparse representations," *Comput. J.*, vol. 52, no. 1, pp. 64–79, Jan. 2009.
- [20] G. Yu, G. Sapiro, and S. Mallat, "Solving inverse problems with piecewise linear estimators: From Gaussian mixture models to structured sparsity," *IEEE Trans. Image Process.*, vol. 21, no. 5, pp. 2481–2499, May 2012.
- [21] I. Ram, M. Elad, and I. Cohen, "Image processing using smooth ordering of its patches," *IEEE Trans. Image Process.*, vol. 22, no. 7, pp. 2764–2774, Jul. 2013.
- [22] A. A. Efros and T. K. Leung, "Texture synthesis by non-parametric sampling," in *Proc. 7th IEEE Int. Conf. Comput. Vis.*, vol. 2, Sep. 1999, pp. 1033–1038.
- [23] M. Bertalmio, L. Vese, G. Sapiro, and S. Osher, "Simultaneous structure and texture image inpainting," *IEEE Trans. Image Process.*, vol. 12, no. 8, pp. 882–889, Aug. 2003.
- [24] A. Criminisi, P. Pérez, and K. Toyama, "Region filling and object removal by exemplar-based image inpainting," *IEEE Trans. Image Process.*, vol. 13, no. 9, pp. 1200–1212, Sep. 2004.
- [25] A. Wong and J. Orchard, "A nonlocal-means approach to exemplar-based inpainting," in *Proc. 15th IEEE Int. Conf. Image Process. (ICIP)*, Oct. 2008, pp. 2600–2603.
- [26] Z. Xu and J. Sun, "Image inpainting by patch propagation using patch sparsity," *IEEE Trans. Image Process.*, vol. 19, no. 5, pp. 1153–1165, May 2010.
- [27] F. Cao, Y. Gousseau, S. Masnou, and P. Pérez, "Geometrically guided exemplar-based inpainting," *SIAM J. Imag. Sci.*, vol. 4, no. 4, pp. 1143–1170, 2011.
- [28] P. Arias, G. Facciolo, V. Caselles, and G. Sapiro, "A variational framework for exemplar-based image inpainting," *Int. J. Comput. Vis.*, vol. 93, no. 3, pp. 319–347, 2011.
- [29] L. I. Rudin, S. Osher, and E. Fatemi, "Nonlinear total variation based noise removal algorithms," *Phys. D, Nonlinear Phenomena*, vol. 60, nos. 1–4, pp. 259–268, 1992.
- [30] A. Beck and M. Teboulle, "A fast iterative shrinkage-thresholding algorithm for linear inverse problems," *SIAM J. Imag. Sci.*, vol. 2, no. 1, pp. 183–202, 2009.
- [31] T. Goldstein and S. Osher, "The split Bregman method for L1-regularized problems," *SIAM J. Imag. Sci.*, vol. 2, no. 2, pp. 323–343, 2009.
- [32] D. L. Donoho, "De-noising by soft-thresholding," *IEEE Trans. Inf. Theory*, vol. 41, no. 3, pp. 613–627, May 1995.
- [33] G. Yu and G. Sapiro, "DCT image denoising: A simple and effective image denoising algorithm," *Image Process. On Line*, vol. 1, 2011. [Online.] Available: <http://dx.doi.org/10.5201/ipol.2011.ys-dct>
- [34] J.-L. Starck, E. J. Candès, and D. L. Donoho, "The curvelet transform for image denoising," *IEEE Trans. Image Process.*, vol. 11, no. 6, pp. 670–684, Jul. 2002.
- [35] M. N. Do and M. Vetterli, "The contourlet transform: An efficient directional multiresolution image representation," *IEEE Trans. Image Process.*, vol. 14, no. 12, pp. 2091–2106, Dec. 2005.
- [36] J.-F. Cai, R. H. Chan, and M. Nikolova, "Two-phase approach for deblurring images corrupted by impulse plus Gaussian noise," *Inverse Problems Imag.*, vol. 2, no. 2, pp. 187–204, 2008.
- [37] X. Bresson, S. Esedoğlu, P. Vanderghyest, J.-P. Thiran, and S. Osher, "Fast global minimization of the active contour/snake model," *J. Math. Imag. Vis.*, vol. 28, no. 2, pp. 151–167, 2007.
- [38] K. Bredies and D. A. Lorenz, "Iterated hard shrinkage for minimization problems with sparsity constraints," *SIAM J. Sci. Comput.*, vol. 30, no. 2, pp. 657–683, 2008.
- [39] M. Elad, B. Matalon, and M. Zibulevsky, "Image denoising with shrinkage and redundant representations," in *Proc. IEEE Comput. Soc. Conf. Comput. Vis. Pattern Recognit.*, vol. 2, Jun. 2006, pp. 1924–1931.
- [40] M. Elad and M. Aharon, "Image denoising via sparse and redundant representations over learned dictionaries," *IEEE Trans. Image Process.*, vol. 15, no. 12, pp. 3736–3745, Dec. 2006.
- [41] S. Hawe, M. Kleinstuber, and K. Diepold, "Analysis operator learning and its application to image reconstruction," *IEEE Trans. Image Process.*, vol. 22, no. 6, pp. 2138–2150, Jun. 2013.
- [42] K. Dabov, A. Foi, V. Katkovnik, and K. Egiazarian, "Image denoising by sparse 3-D transform-domain collaborative filtering," *IEEE Trans. Image Process.*, vol. 16, no. 8, pp. 2080–2095, Aug. 2007.
- [43] A. Danielyan, V. Katkovnik, and K. Egiazarian, "BM3D frames and variational image deblurring," *IEEE Trans. Image Process.*, vol. 21, no. 4, pp. 1715–1728, Apr. 2012.
- [44] Y.-W. Wen, M. K. Ng, and W.-K. Ching, "Iterative algorithms based on decoupling of deblurring and denoising for image restoration," *SIAM J. Sci. Comput.*, vol. 30, no. 5, pp. 2655–2674, 2008.
- [45] J. Nocedal and S. J. Wright, *Penalty and Augmented Lagrangian Methods*. New York, NY, USA: Springer-Verlag, 2006.
- [46] D. P. Bertsekas, A. Nedić, and A. E. Ozdaglar, *Convex Analysis and Optimization*. Belmont, CA, USA: Athena Scientific, 2003.
- [47] Y. Wang, J. Yang, W. Yin, and Y. Zhang, "A new alternating minimization algorithm for total variation image reconstruction," *SIAM J. Imag. Sci.*, vol. 1, no. 3, pp. 248–272, 2008.
- [48] R. A. Horn and C. R. Johnson, *Matrix Analysis*. Cambridge, U.K.: Cambridge Univ. Press, 2012.



Fang Li received the M.Sc. degree in mathematics from South West China Normal University, Chongqing, China, in 2004, and the Ph.D. degree in mathematics from East China Normal University, Shanghai, China, in 2007. She has been with the Department of Mathematics, East China Normal University, since 2007, where she is currently an Associate Professor. Her research interests include anisotropic diffusion filtering, the variational methods, and PDEs in image processing.



Tiejong Zeng received the B.S. degree from Peking University, Beijing, China, in 2000, the M.S. degree from Ecole Polytechnique, Paris, France, in 2004, and the Ph.D. degree from the University of Paris XIII, Paris, in 2007. Before joining Hong Kong Baptist University, Kowloon Tong, China, as an Assistant Professor, he was a Post-Doctoral Researcher with the Centre de Mathématiques et de Leurs Applications, ENS de Cachan, Cachan, France. His research interests are image processing, statistical learning, and scientific computing.